Supporting Information

A General Strategy to Fabricate Porous Co-Based Bimetallic Metal Oxides Nanosheets for High Performance CO Sensing

Cong Qin[1], Bing Wang[1,], Nan Wu[2], Cheng Han[1], Yingde Wang[1,*]*

[1]Science and Technology on Advanced Ceramic Fibers and Composites Laboratory, College of Aerospace Science and Engineering, National University of Defense Technology, Changsha 410073, PR China

[2]Department of Material Science and Engineering, College of Aerospace Science and Engineering, National University of Defense Technology, Changsha 410073, PR China

*Corresponding authors:

E-Mail: bingwang@nudt.edu.cn

E-Mail: wangyingde@nudt.edu.cn

Contents

Note S1 Reagents.

Cobalt nitrate hexahydrate ($Co(NO_3)_2 \cdot 6H_2O$, 99.0%), zinc nitrate hexahydrate ($Zn(NO_3)_2 \cdot 6H_2O$, 99.0%), copper nitrate trihydrate ($Cu(NO_3)_2 \cdot 3H_2O$, 99.0%), manganese nitrate hexahydrate ($Mn(NO_3)_2 \cdot 6H_2O$), nickel nitrate hexahydrate ($Ni(NO_3)_2 \cdot 6H_2O$, 98.0%), anhydrous methanol (99.5%) and 2-methylimidazole (2-mIM, 99.0%) were purchased from Aladdin Industrial, Inc. (Shanghai, China). All chemicals were used without further purification.

Note S2 Characterization.

X-ray diffraction (XRD) pattern was obtained using a PANalytical Empyrean with a Cu Kα radiation (0.15406 nm). The morphology and microstructure of the products were observed by field emission scanning electron microscopy (FE-SEM, Hitachi S-4800, Chiyoda, Tokyo, Japan) and transmission electron microscope (TEM, Tecnai G2 F20 S-TWIN). The thermogravimetric analysis (TGA) of the product was measured using a TG209F1 (NETZSCH, Germany). Nitrogen (N_2) adsorption-desorption tests were achieved using a 3H-2000PM2 analyzer. Before measurements, the products were subjected to degassing in vacuum at 200 ^{o}C for 6 h. The chemical binding states of the samples were conducted by X-ray photoelectron spectroscopy (XPS, Thermo Scientific ESCALAB 250Xi).

Note S3 Sensor fabrication and measurement.

Firstly, 2 mg of the as-prepared sample was dispersed in 200 μL of deionized water and sonicated for 0.5 h to form a homogeneous suspension. Then, a resistive sensor was formed by dropping 20 μL of suspension onto an alumina ceramic substrate (10 mm in length, 5 mm and 0.25 mm in width and height, respectively) with Au interdigitated electrodes. The sensor was naturally dried in air and heated at 100 ^{o}C for 2h to ensure a close contact between Au electrodes and sensing materials. The gas-sensing measurement was performed on a CGS-1TPS instrument (Beijing Elite Tech Co., Ltd. Beijing, China). The relative humidity was fixed at 40% RH. For a p-type semiconductor, the response (S) is defined as $(R_g-R_a)/R_a \cdot 100\%$, where R_a and R_g represent the resistances of the sensors in ambient air and CO, respectively. The response/recovery time are defined as the time required for the sensor to reach 90% of the total resistance change in ambient air or CO.

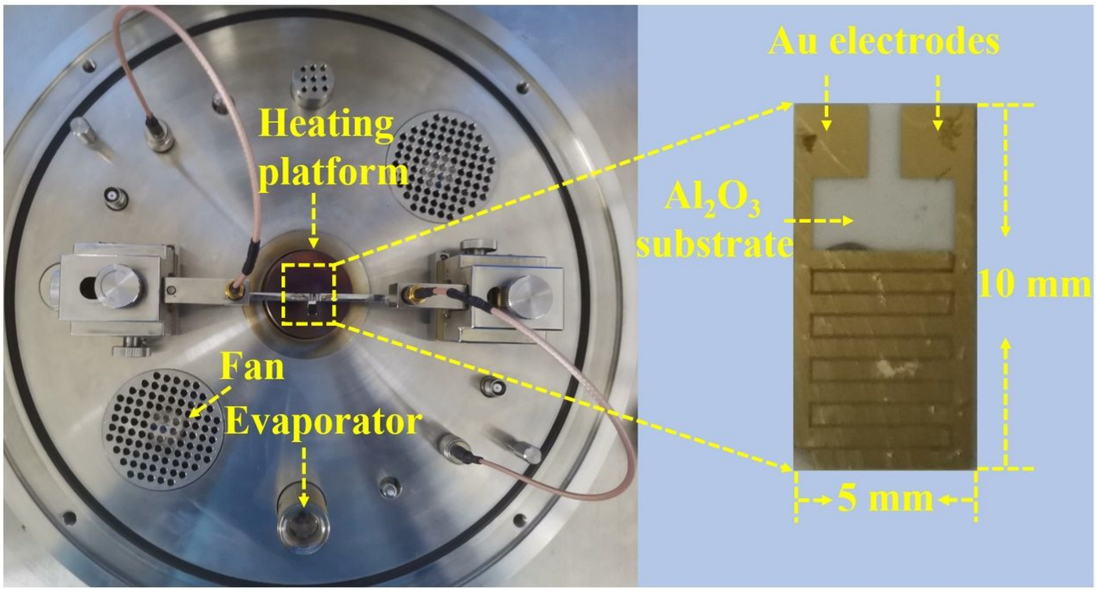

Figure S1. Photograph of the gas sensing measurement system and Au electrodes.

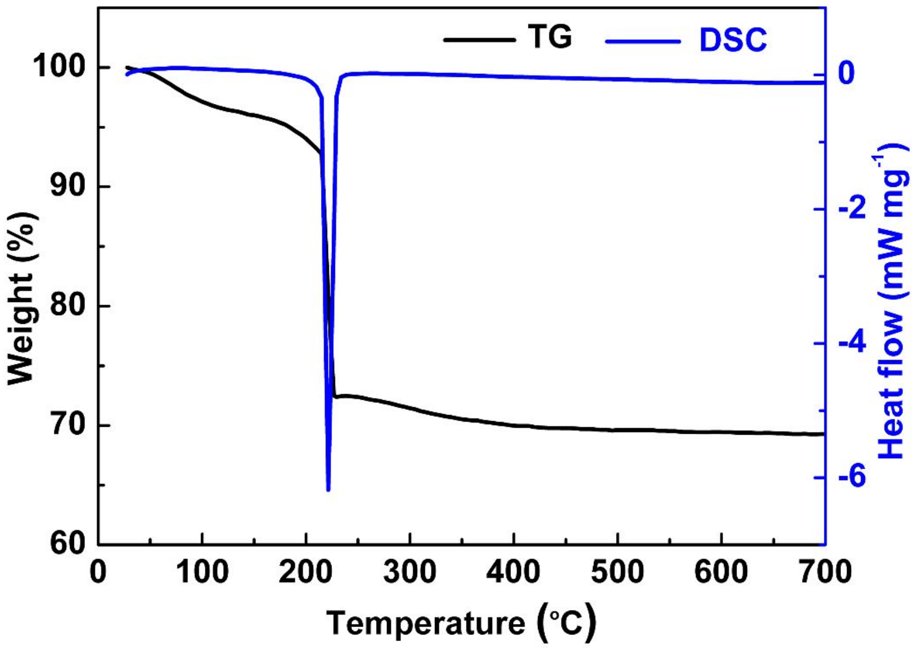

Figure S2. TG-DSC curves of Co-MOF NS.

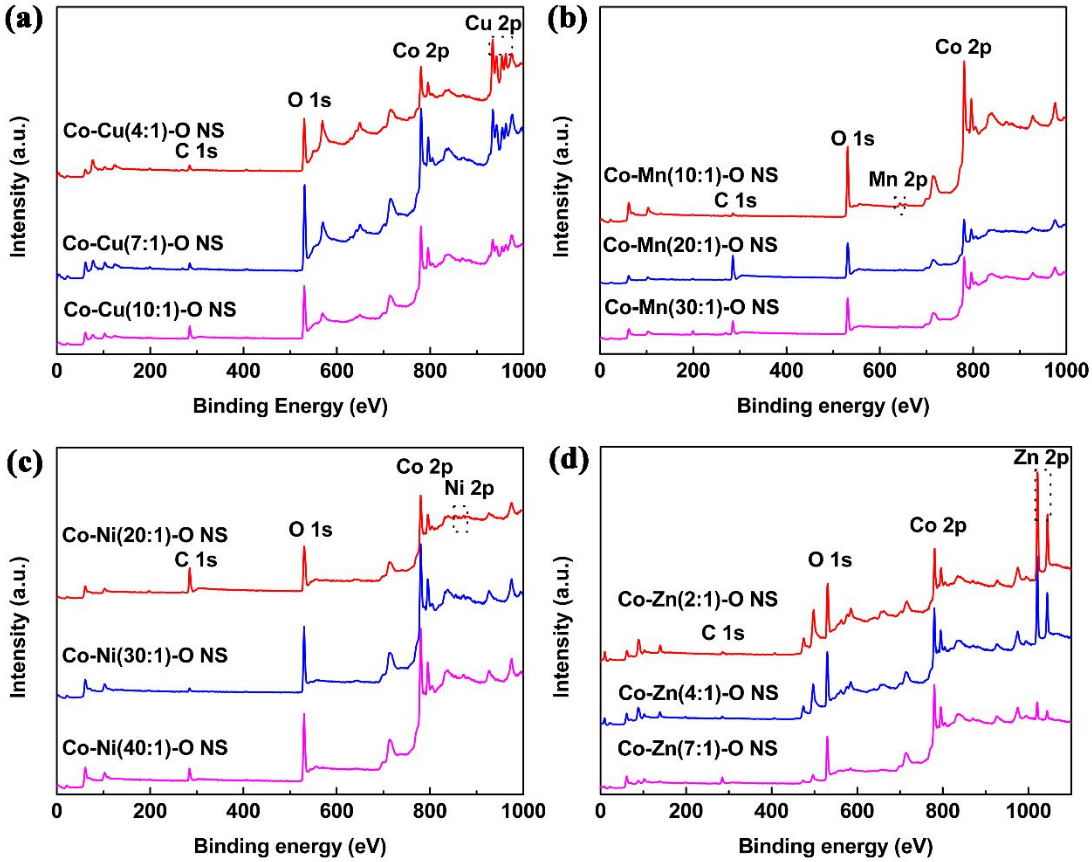

Figure S3. XPS survey spectra of (a) Co-Cu-O NS, (b) Co-Mn-O NS, (c) Co-Ni-O NS, and (d) Co-Zn-O NS.

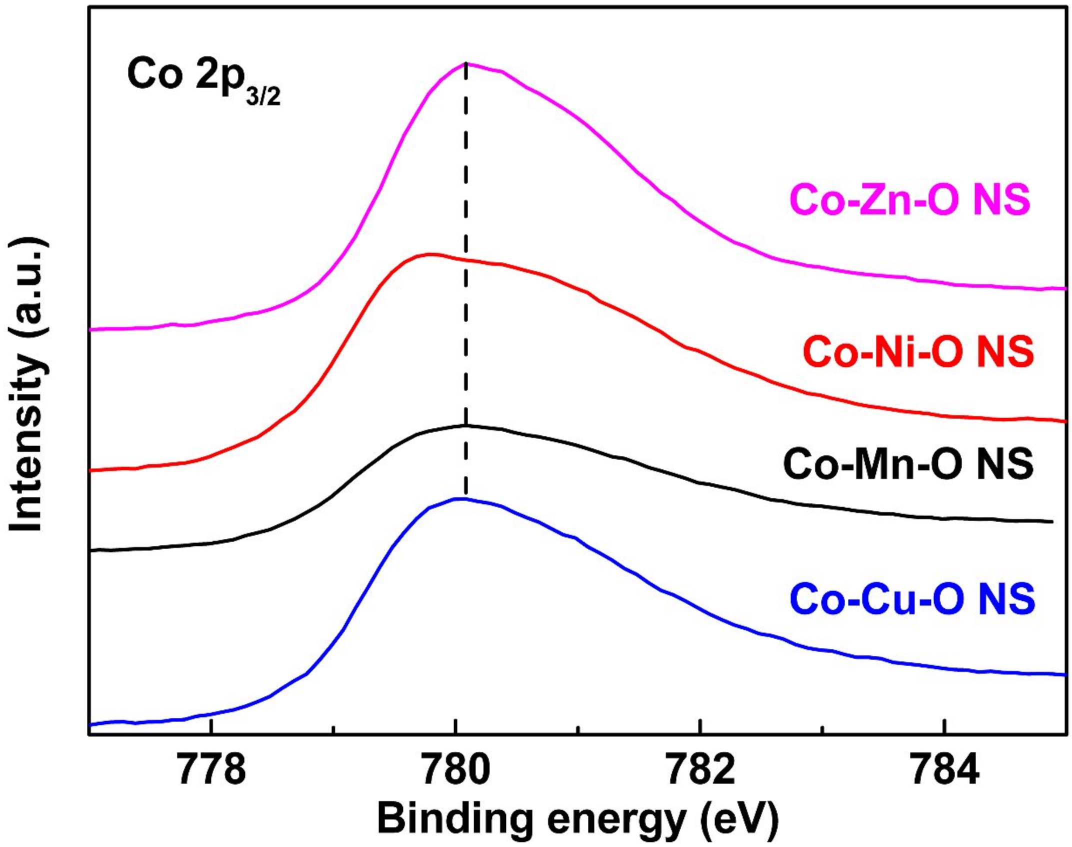

Figure S4. Co $2p_{3/2}$ spectrum of Co-Cu(7:1)-O NS, Co-Mn(20:1)-O NS, Co-Ni(30:1)-O NS and Co-Zn(4:1)-O NS.

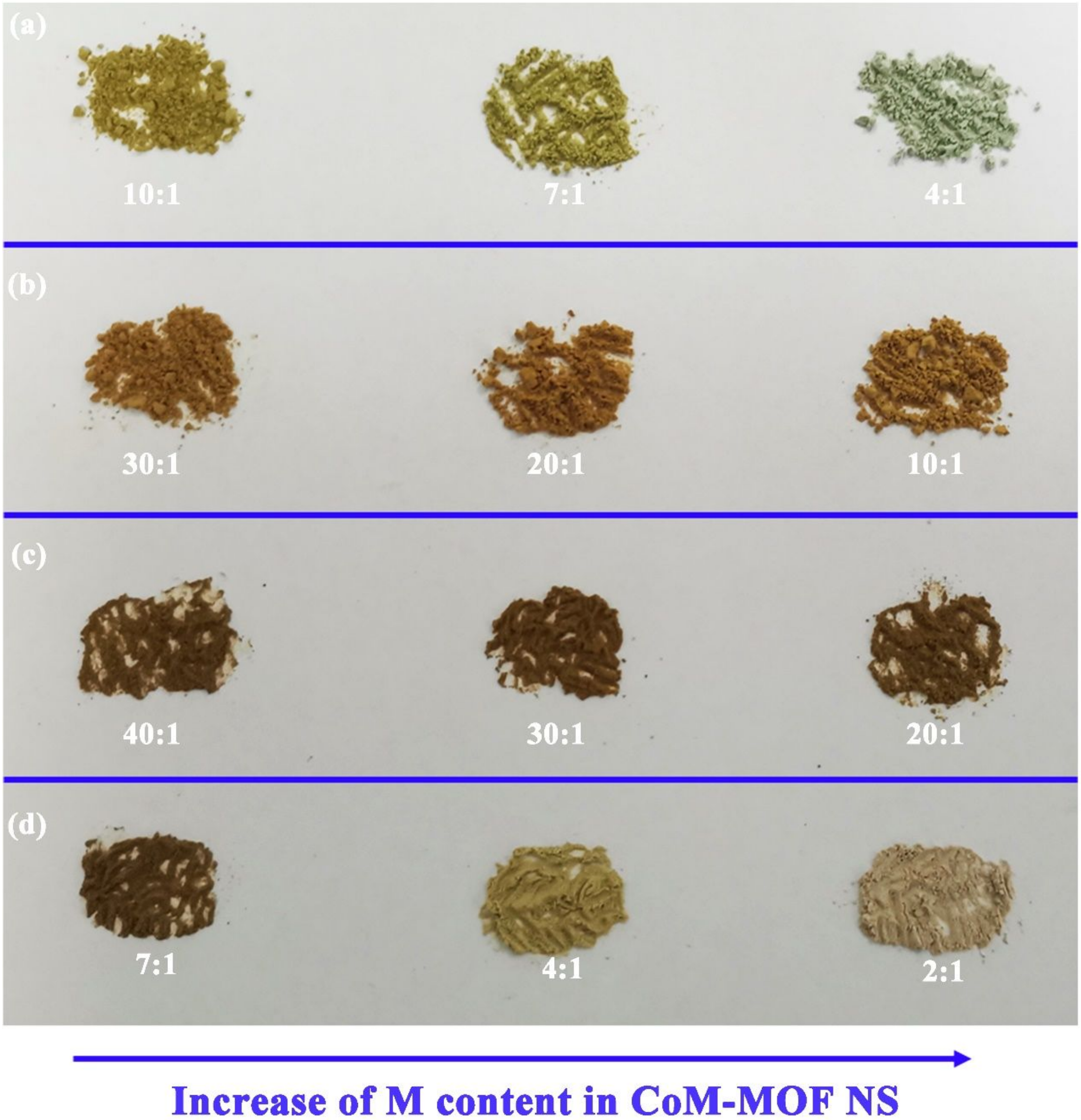

Figure S5. Optical photographs of (a) CoCu-MOF NS, (b) CoMn-MOF NS, (c) CoNi-MOF NS, and (d) CoZn-MOF NS with different Co/M ratios in the initial precursors. Note: In fact, we synthesized a series of samples with different Co/M (M = Cu, Mn, Ni, Zn) ratios for every group. For the sake of discussion, we only picked out three samples from each group according to the sensing-performances for the further statement.

Table S1. ICP-AES analysis results of Co-M-O nanosheets.

Sample	Element	Content (wt.%)
Co-Cu(10:1)-O	Cu	1.16%
Co-Cu(7:1)-O	Cu	2.17%
Co-Cu(4:1)-O	Cu	4.20%
Co-Mn(30:1)-O	Mn	0.08%
Co-Mn(20:1)-O	Mn	0.14%
Co-Mn(10:1)-O	Mn	0.26%
Co-Ni(40:1)-O	Ni	0.20%
Co-Ni(30:1)-O	Ni	0.26%
Co-Ni(20:1)-O	Ni	0.37%
Co-Zn(7:1)-O	Zn	2.28%
Co-Zn(4:1)-O	Zn	11.88%
Co-Zn(2:1)-O	Zn	22.62%

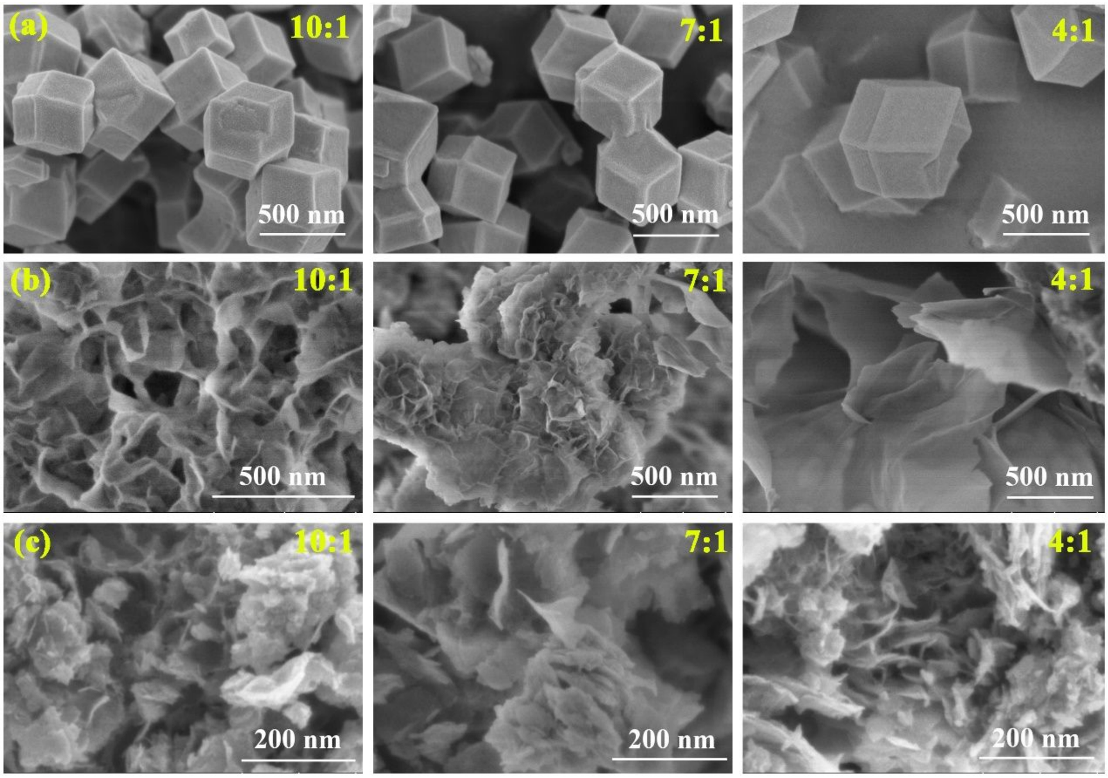

Figure S6. SEM images of the (a) ZIF-CoCu, (b) CoCu-MOF NS, and (c) Co-Cu-O NS with different Co/Cu ratios.

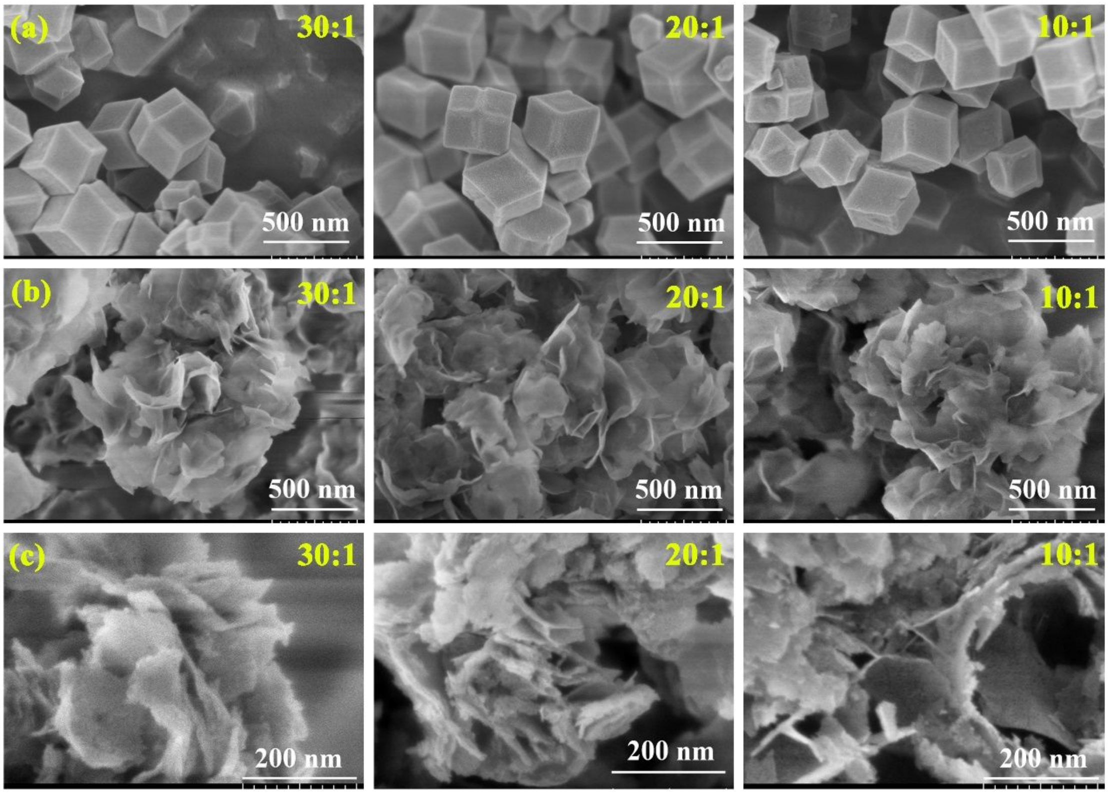

Figure S7. SEM images of the (a) ZIF-CoMn, (b) CoMn-MOF NS, and (c) Co-Mn-O NS with different Co/Mn ratios.

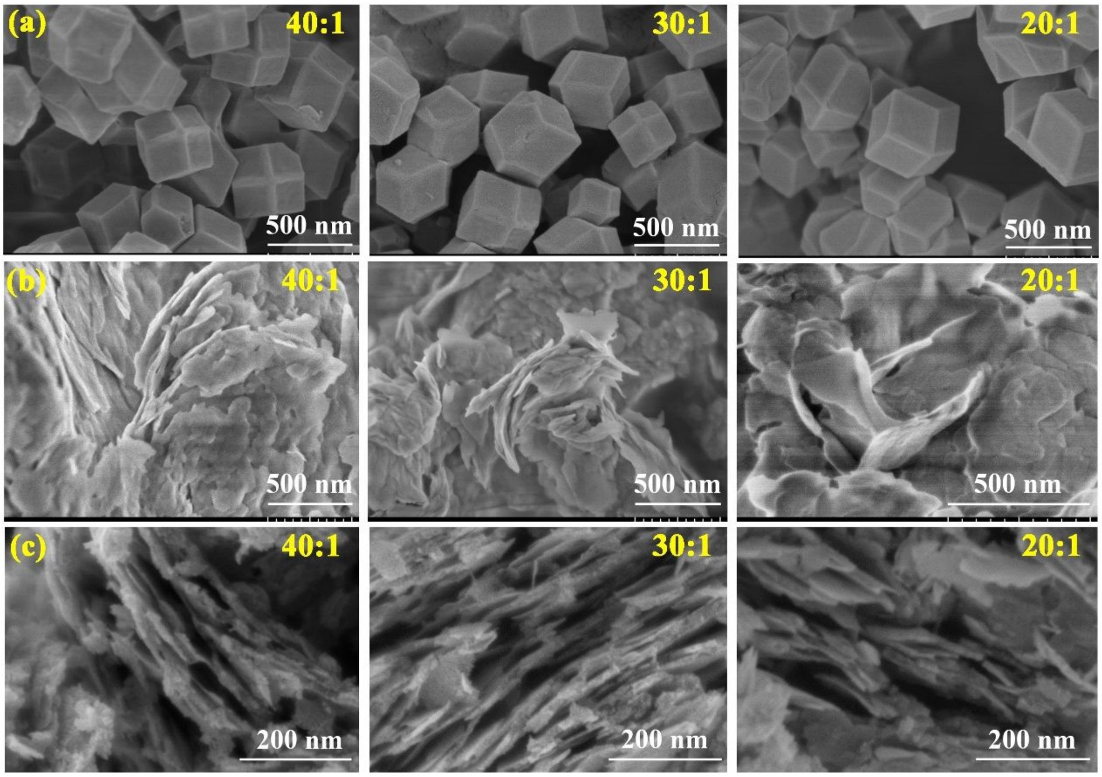

Figure S8. SEM images of the (a) ZIF-CoNi, (b) CoNi-MOF NS, and (c) Co-Ni-O NS with different Co/Ni ratios.

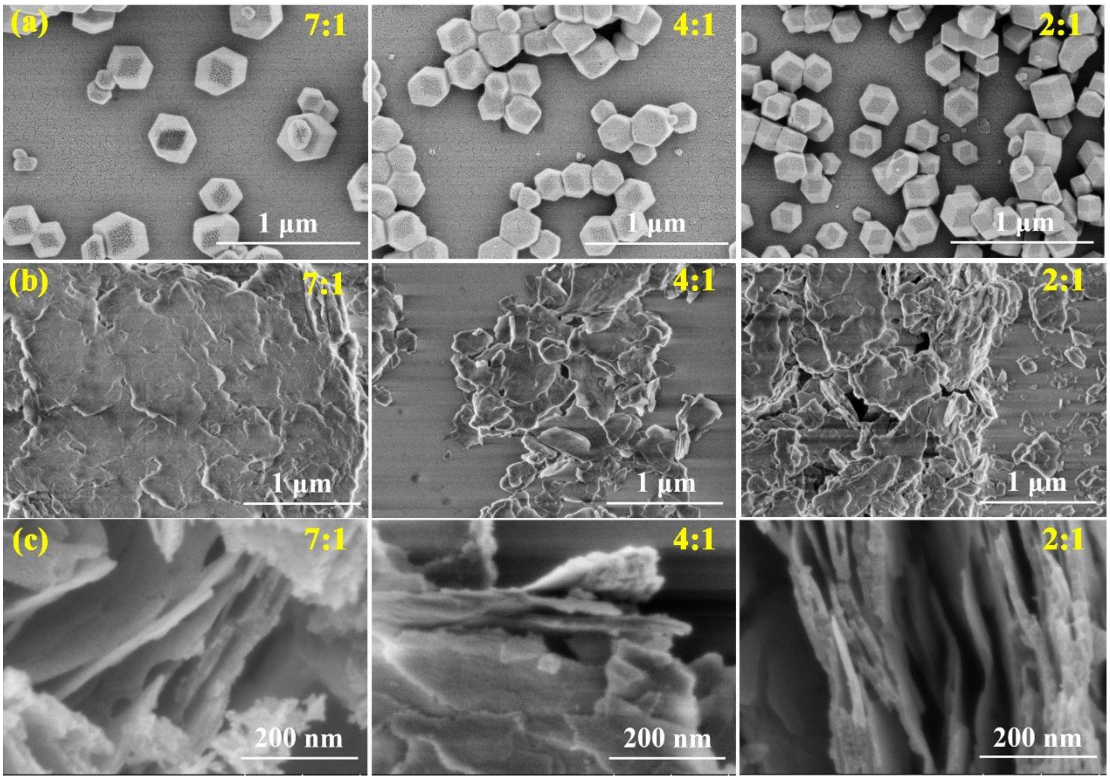

Figure S9. SEM images of the (a) ZIF-CoZn, (b) CoZn-MOF NS, and (c) Co-Zn-O NS with different Co/Zn ratios.

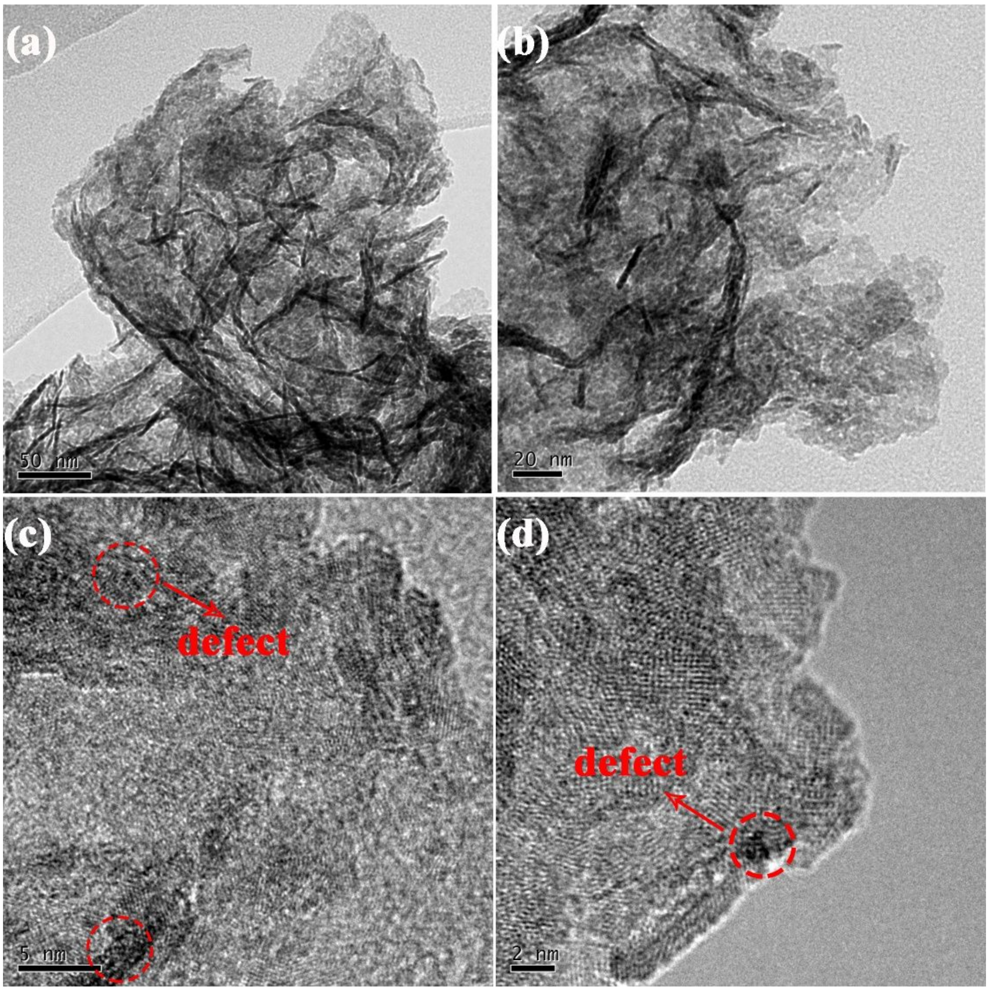

Figure S10. TEM images of the Co-Cu-O NS sample.

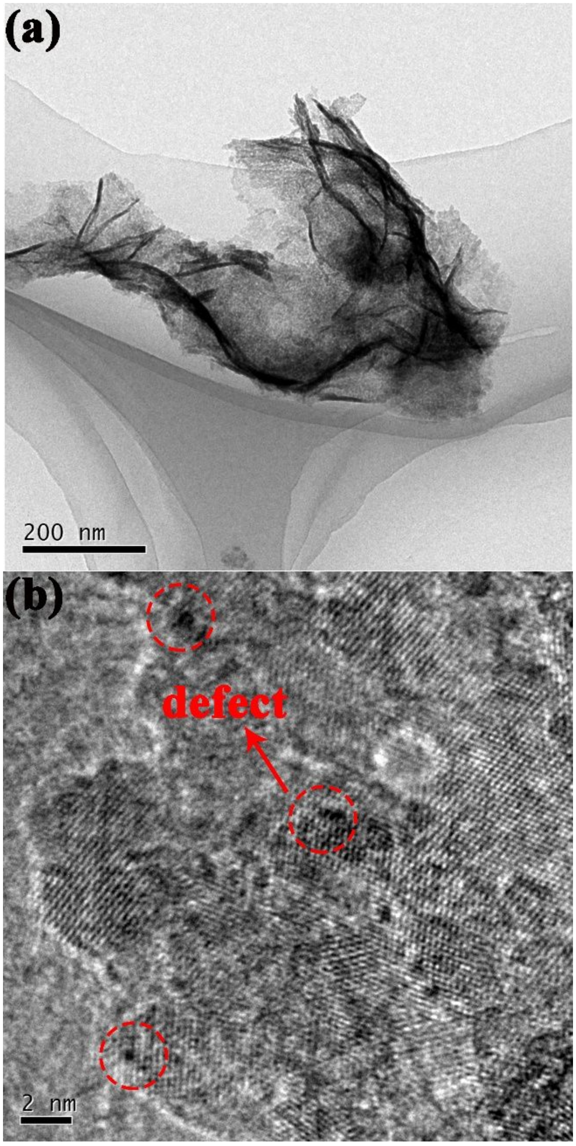

Figure S11. TEM images of the Co-Mn-O NS sample.

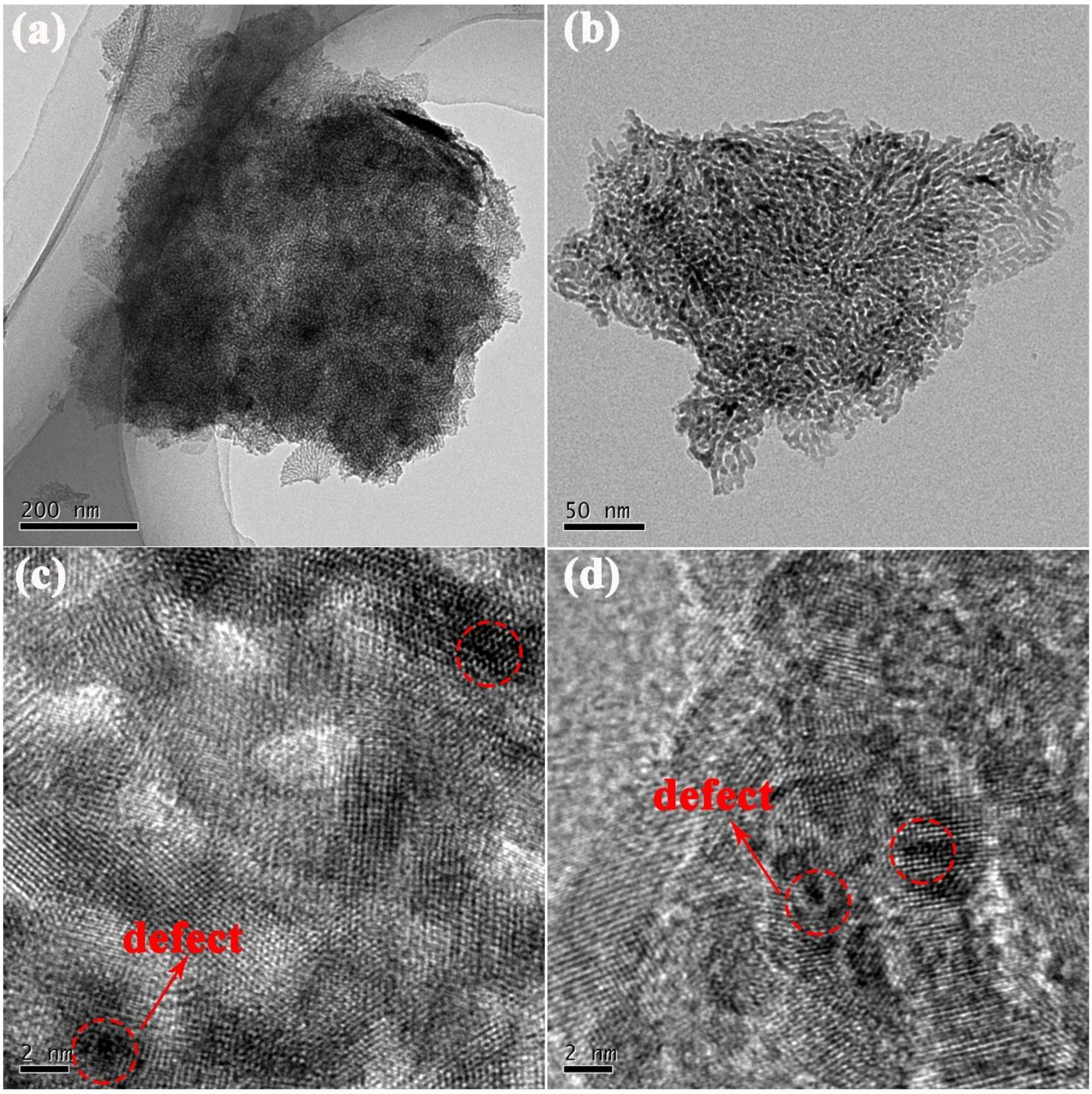

Figure S12. TEM images of the Co-Ni-O NS sample.

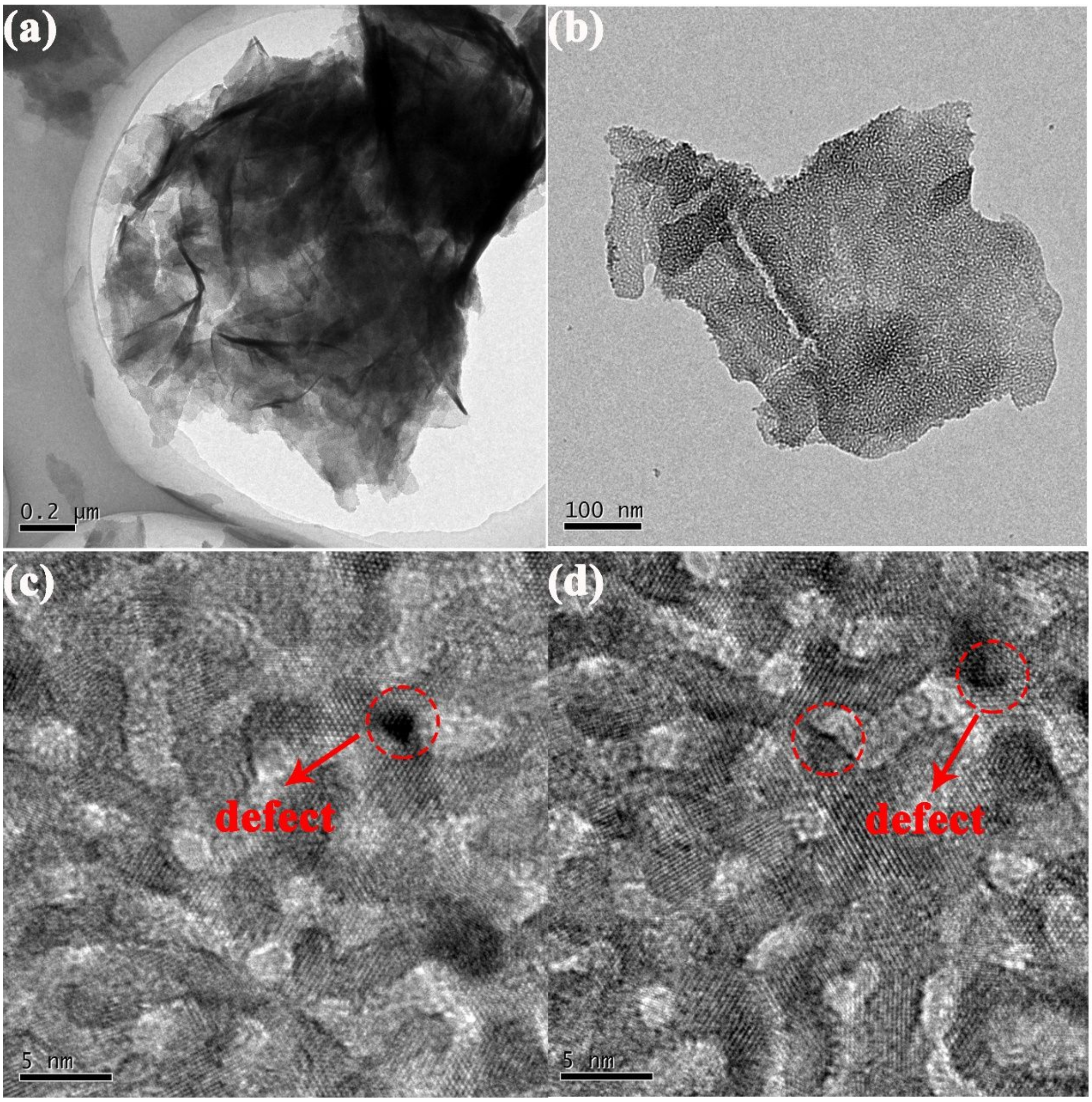

Figure S13. TEM images of the Co-Zn-O NS sample.

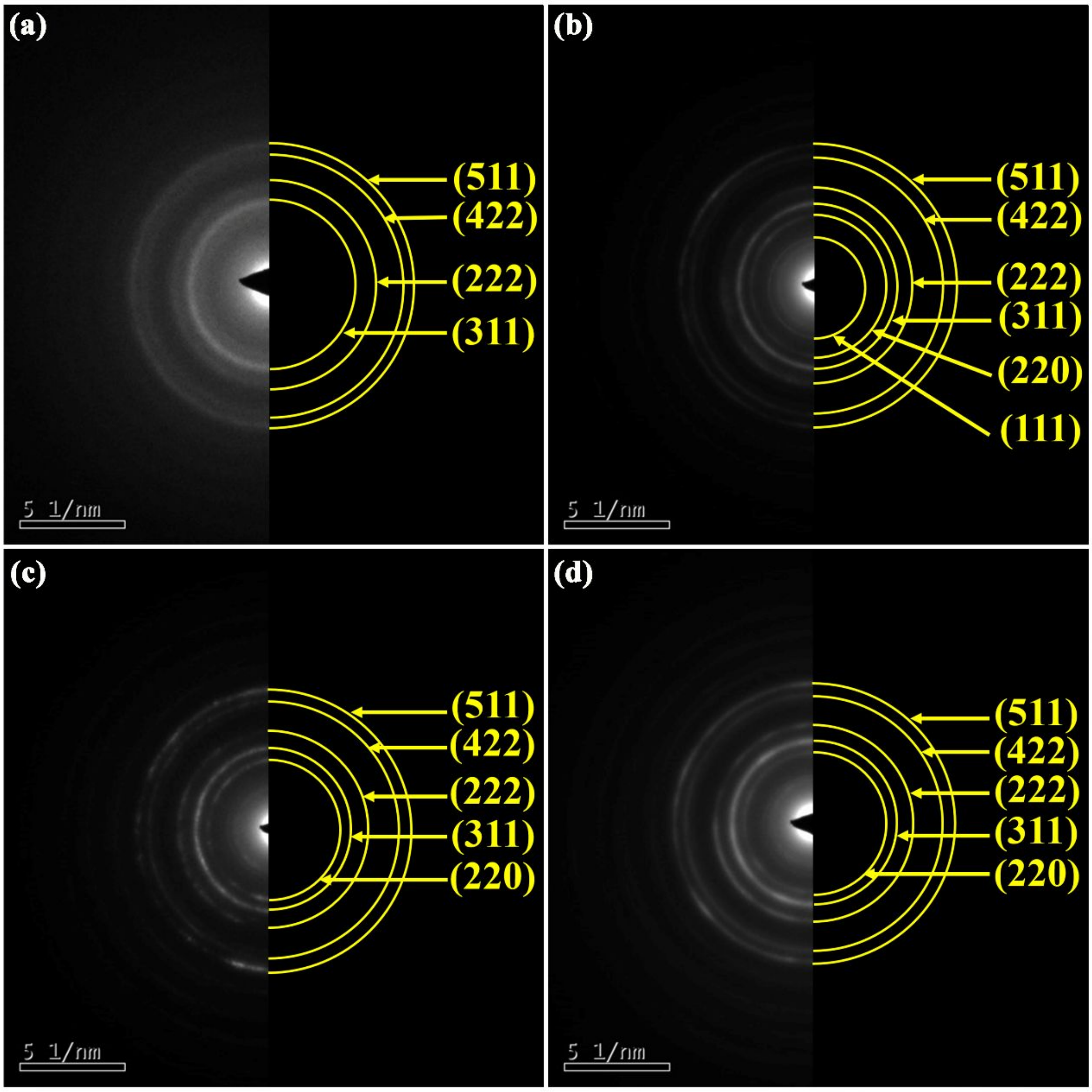

Figure S14. SAED patterns of (a) Co-Cu-O NS, (b) Co-Mn-O NS, (c) Co-Ni-O NS, and (d) Co-Zn-O NS samples.

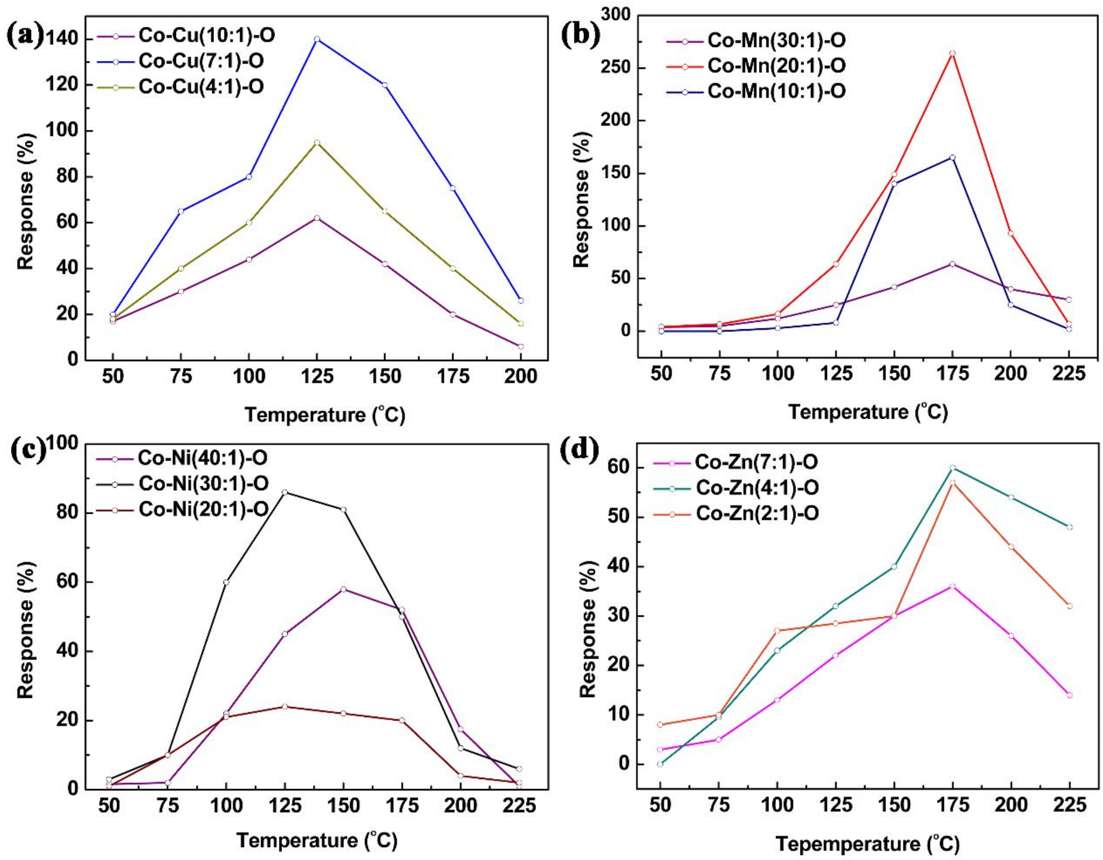

Figure S15. Temperature-dependent sensing response of (a) Co-Cu-O NS, (b) Co-Mn-O NS, (c) Co-Ni-O NS, and (d) Co-Zn-O NS toward 100 ppm of CO.

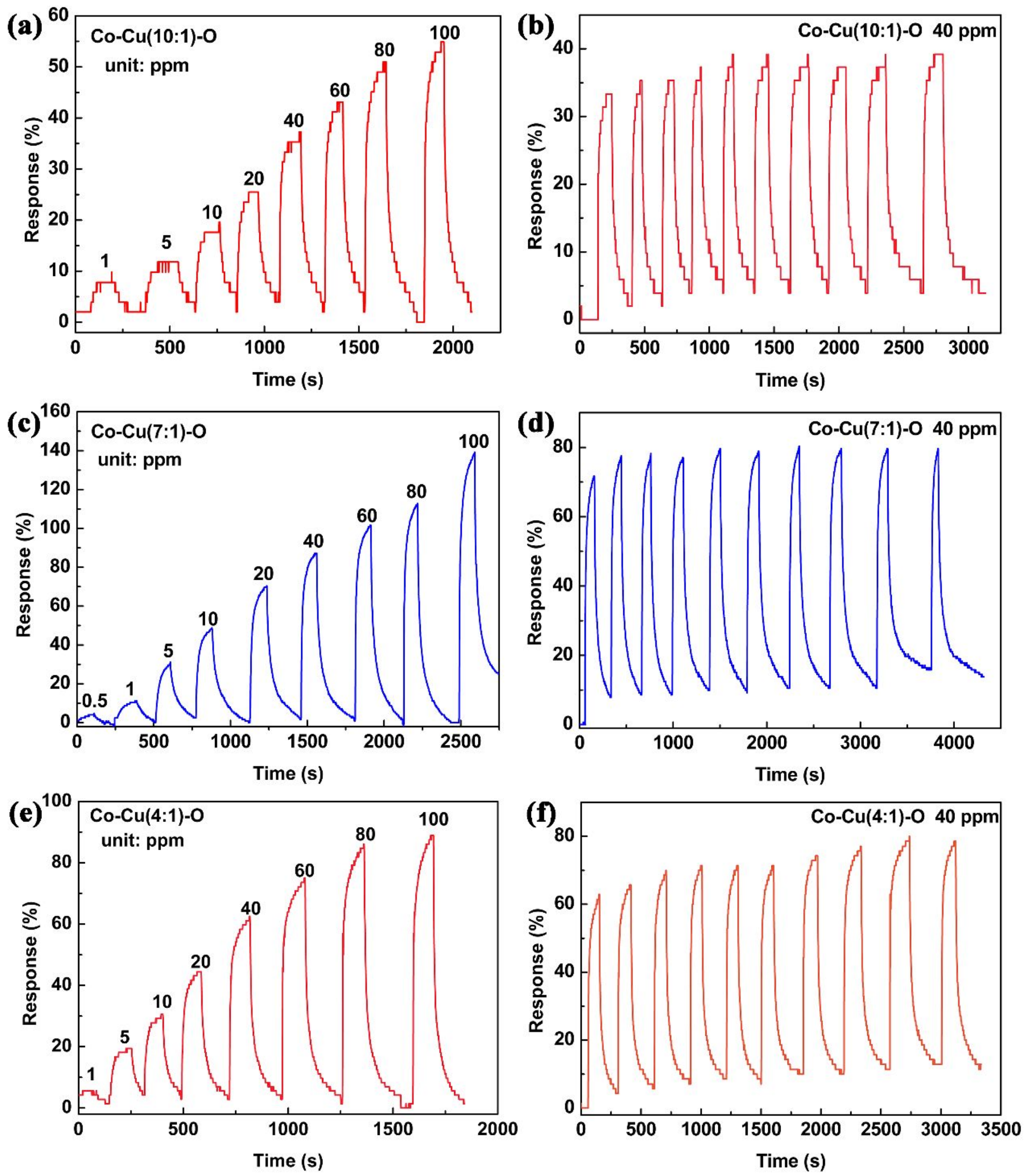

Figure S16. Dynamic sensing response of (a) and (b) Co-Cu(10:1)-O NS toward CO, (c) and (d) Co-Cu(7:1)-O NS toward CO, (e) and (f) Co-Cu(4:1)-O NS toward CO at 125 ^{o}C.

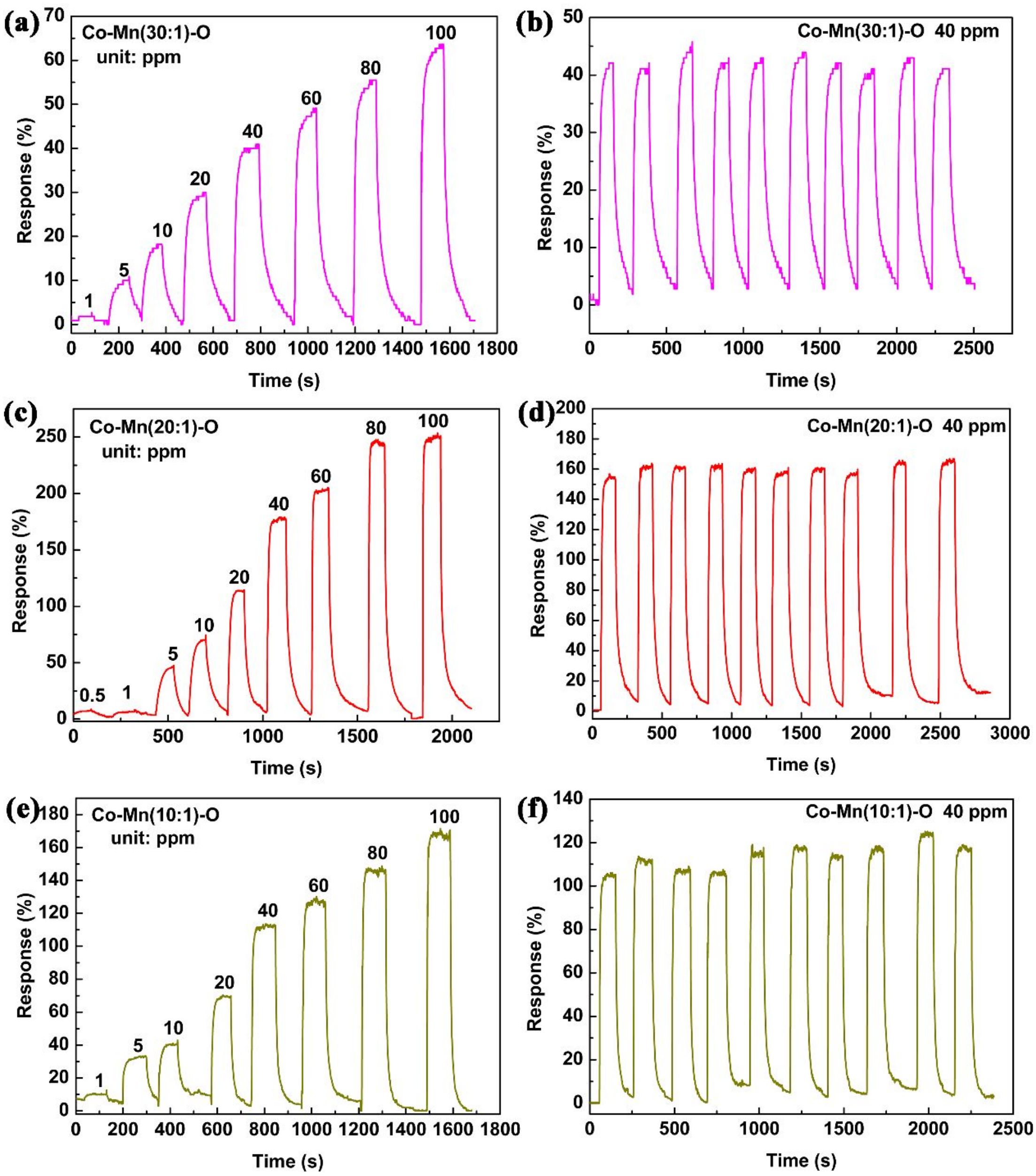

Figure S17. Dynamic sensing response of (a) and (b) Co-Mn(30:1)-O NS toward CO, (c) and (d) Co-Mn(20:1)-O NS toward CO, (e) and (f) Co-Mn(10:1)-O NS toward CO at 175 ^{o}C.

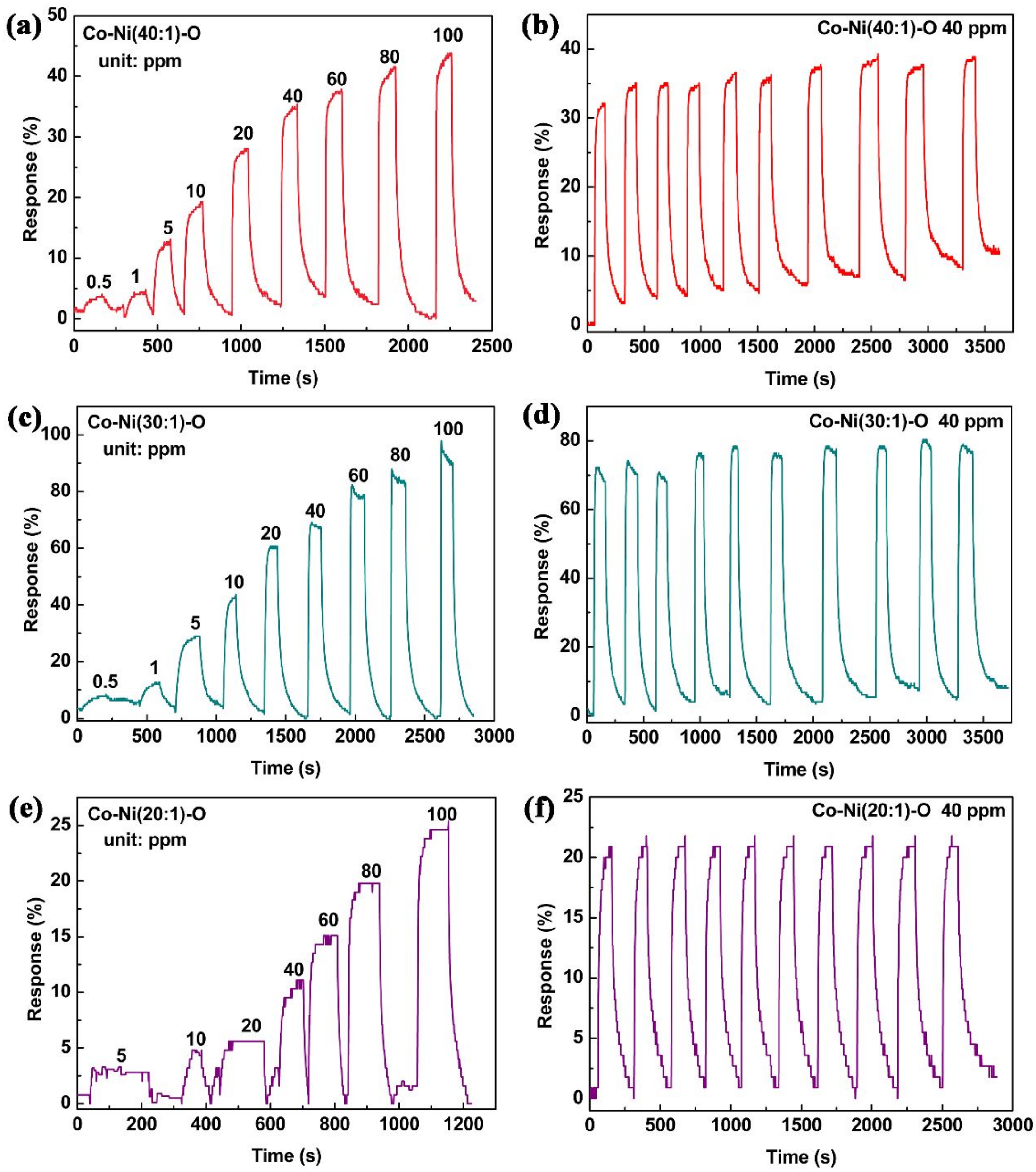

Figure S18. Dynamic sensing response of (a) and (b) Co-Ni(40:1)-O NS toward CO, (c) and (d) Co-Ni(30:1)-O NS toward CO, (e) and (f) Co-Ni(20:1)-O NS toward CO at 125 ^{o}C.

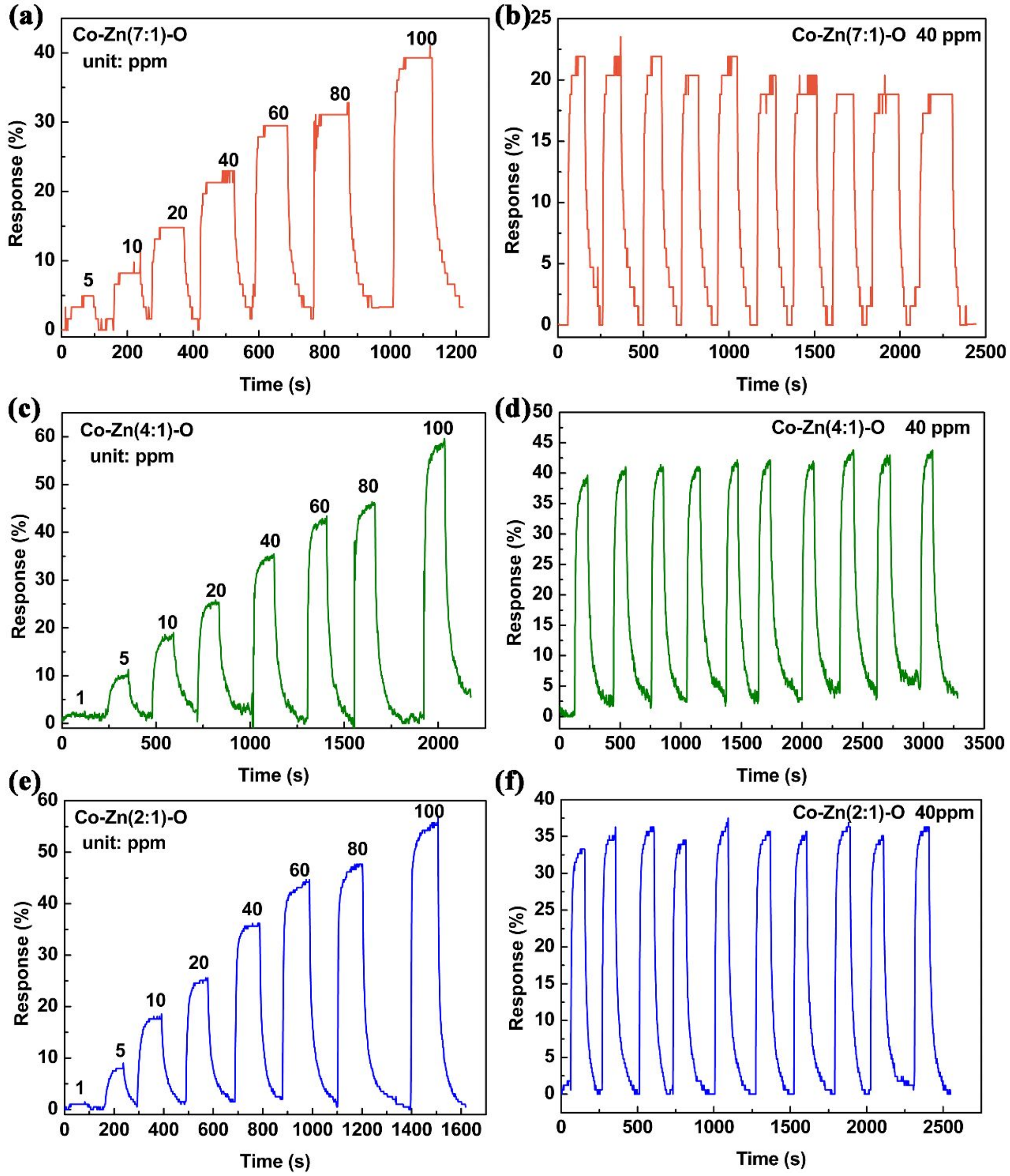

Figure S19. Dynamic sensing response of (a) and (b) Co-Zn(7:1)-O NS toward CO, (c) and (d) Co-Zn(4:1)-O NS toward CO, (e) and (f) Co-Zn(2:1)-O NS toward CO at 175 ^{o}C.

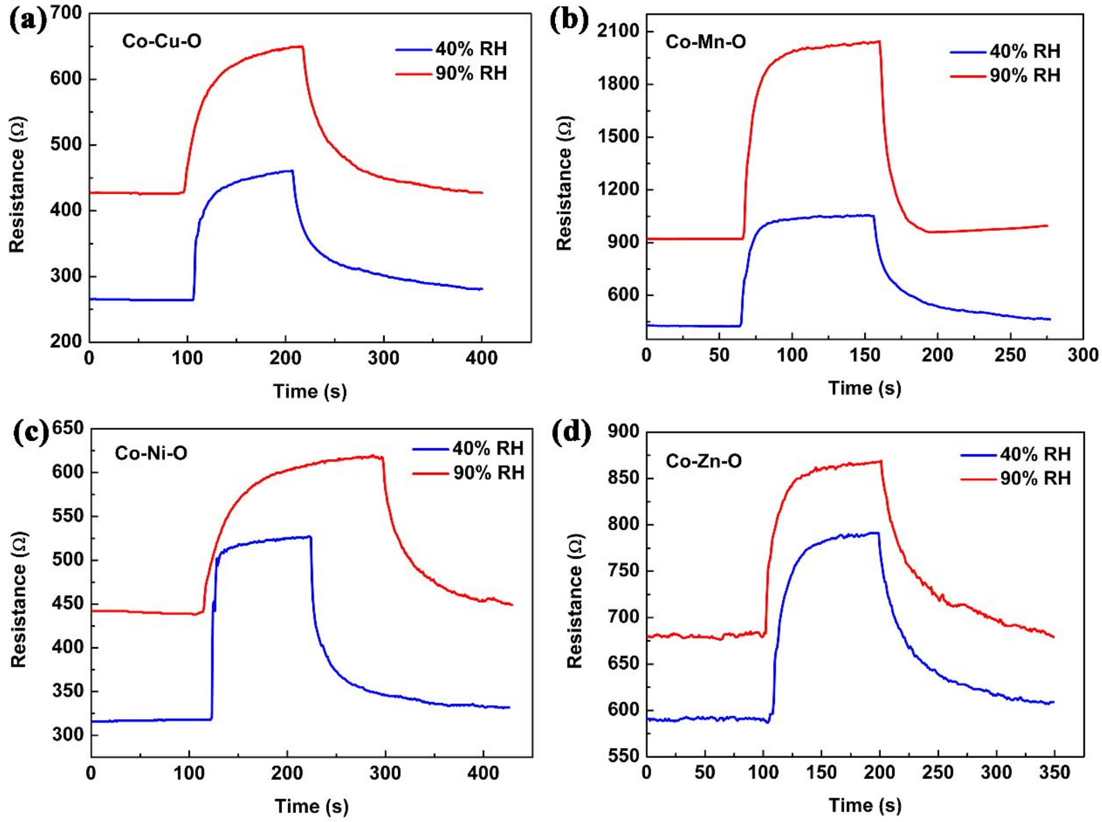

Figure S20. Dynamic gas-sensing transients of the (a) Co-Cu-O toward 40 ppm of CO at 125 ^{o}C, (b) Co-Mn-O toward 40 ppm of CO at 175 ^{o}C, (c) Co-Ni-O toward 40 ppm of CO at 125 ^{o}C, and (d) Co-Zn-O toward 40 ppm of CO at 175 ^{o}C, respectively, under different humid (40% RH and 90% RH) conditions.

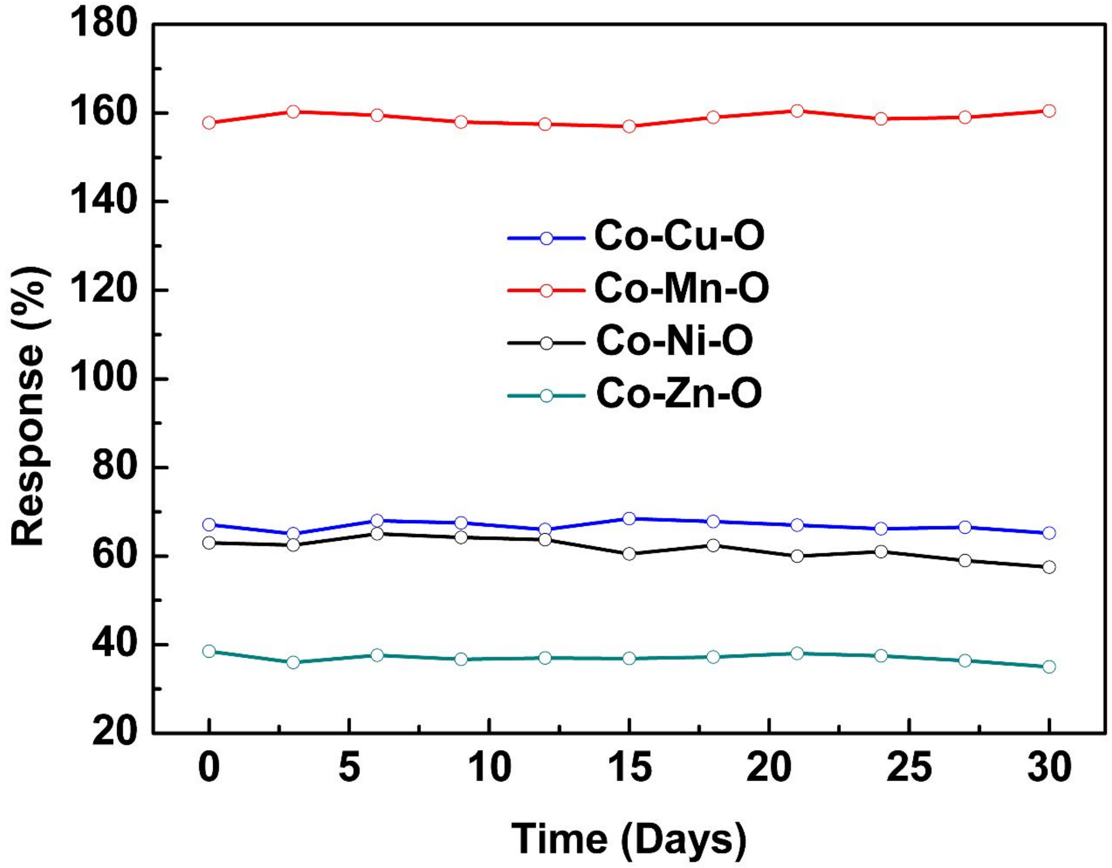

Figure S21. Long-term stability of the sensors toward 40 ppm CO of Co-Cu-O and Co-Ni-O at 125 ^{o}C, Co-Mn-O and Co-Zn-O at 175 ^{o}C.

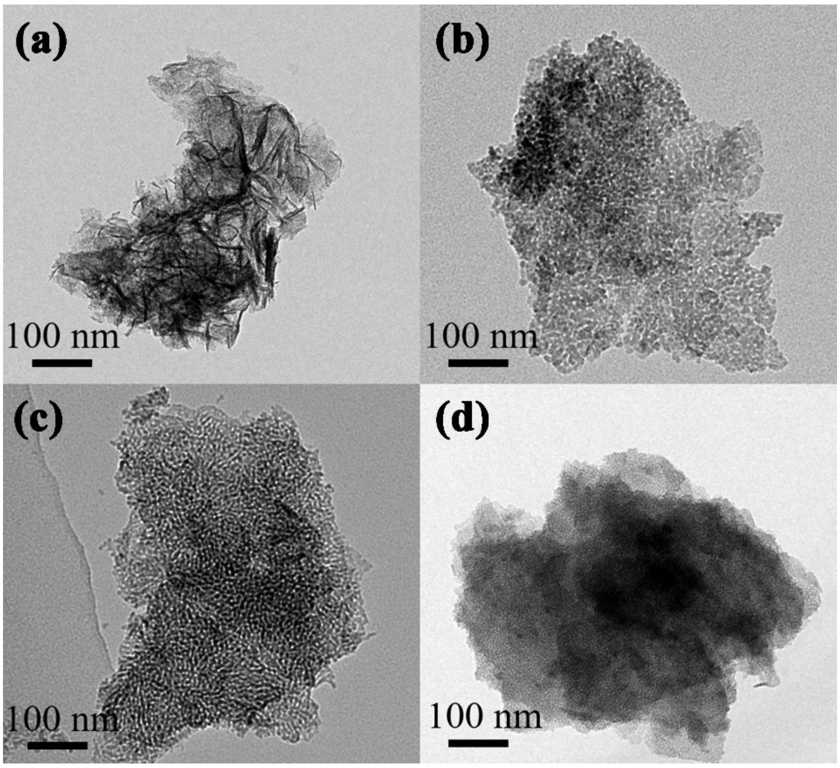

Figure S22. TEM images of the Co-M-O NS samples: (a) Co-Cu-O; (b) Co-Mn-O; (c) Co-Ni-O; (d) Co-Zn-O after humidity and stability tests to CO.

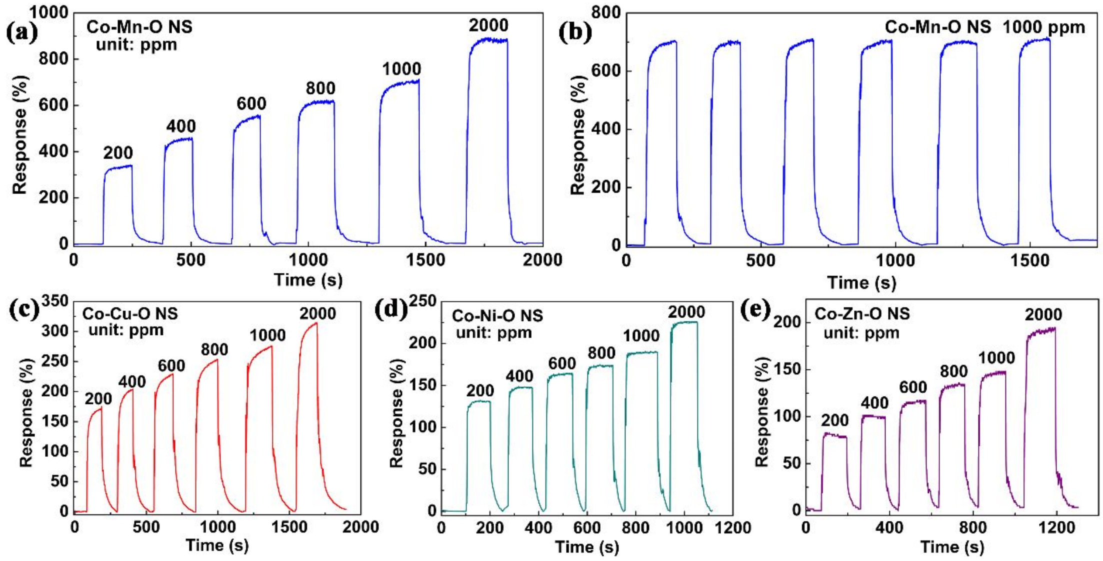

Figure S23. Dynamic sensing response of (a) and (b) Co-Mn-O NS at 175 ^{o}C, (c) Co-Cu-O NS at 125 ^{o}C, (d) Co-Ni-O NS at 125 ^{o}C, (e) Co-Zn-O NS at 175 ^{o}C.

Table S2. Comparison of carbon monoxide sensing performances of Co_3O_4-based materials reported in literature and in this work.

Sensing Materials	Con. (ppm)	Res.	Tem. (^oC)	t_{res}/t_{rec} (s)	Ref.
Co_3O_4 nanofibers	40	3.6^a	100	N/A	(1)
Co_3O_4/TiO_2 nanofibers	80	15.5^a	220	0.5 s/1 s	(2)
Co_3O_4 nano-combs	100	11.6^a	180	0.5 s/2.3 s	(3)
Co_3O_4 nanospheres	25	< 2.2^a	200	N/A	(4)
Co_3O_4/Al-ZnO nanoparticles	1000	0.8%^{b}	160	N/A	(5)
Ag/Co_3O_4 nanoparticles	800	85%^{b}	130	N/A	(6)
PANI/Co_3O_4 nanoparticles	75	81%^{b}	RT	40 s/N/A	(7)
Co_3O_4 nanorods	50	6.55^a	250	4 s/6 s	(8)
NiO/Co_3O_4 nanoparticles	300	150%^{b}	150	N/A	(9)
Co_3O_4 nanpspheres	300	1.57^a	170	N/A	(10)
Co_3O_4 nanowires	50	12^a	100	N/A	(11)
Co-Cu-O NS	100	140%^{b}	125	21 s/80 s	This work
Co-Mn-O NS	100	264%^{b}	175	10 s/53 s	This work
Co-Ni-O NS	100	90%^{b}	125	4 s/68 s	This work
Co-Zn-O NS	100	60%^{b}	175	27 s/80 s	This work

Note: a: (R_g/R_a), b: (R_g-R_a)/R_a*100%, Con: Concentration, Res: Response, Tem: Temperature

Table S3. Results of curve fitting of Co 2p and O 1s XPS spectra of the Co-M-O samples

Sensing Materials	Co^{3+}/Co^{2+}	O_L (%)	O_V (%)	O_C (%)
Co-Cu-O NS	2.35	44.5	25.9	29.6
Co-Mn-O NS	2.60	42.3	22.6	35.1
Co-Ni-O NS	2.21	45.1	27.9	27.0
Co-Zn-O NS	1.30	60.1	15.2	24.7

References

(1) Busacca, C.; Donato, A.; Faro, M. L.; Malara, A.; Neri, G.; Trocino, S. CO gas sensing performance of electrospun Co_3O_4 nanostructures at low operating temperature. Sens. Actuators B: Chem. 2020, 303, 127193.

(2) Wang, L. L.; Deng, J. N.; Lou, Z.; Zhang, T. Cross-linked p-type Co_3O_4 octahedral nanoparticles in 1D n-type TiO_2 nanofibers for high-performance sensing devices. J. Mater. Chem. A 2014, 2, 10022-10028.

(3) Deng, J. N.; Wang, L. L.; Lou, Z.; Zhang, T. Fast response/recovery performance of comb-like Co_3O_4 nanostructure. RSC Adv. 2014, 4, 21115-21120.

(4) Vetter, S.; Haffer, S.; Wagner, T.; Tiemann, M. Nanostructured Co_3O_4 as a CO gas sensor: Temperature-dependent behavior. Sens. Actuators B: Chem. 2015, 206, 133-138.

(5) Fort, A.; Panzardi, E.; Vegnoli, V.; Hjiri, M.; Aida, M. S.; Mugnaini, M.; Addabbo, T. Co_3O_4/Al-ZnO Nano-composites: Gas Sensing Properties. Sens. 2019, 19, 760.

(6) Molavi, R.; Sheikhi, M. H.; Low temperature carbon monoxide gas sensor based on Ag-Co_3O_4 thick film nanocomposite. Mater. Lett. 2018, 233, 74-77.

(7) Sen, T.; Shimpi, N. G.; Mishra, S. Room temperature CO sensing by polyaniline/Co_3O_4 nanocomposite. J. Appl. Polym. Sci. 2016, 133, 44115.

(8) Patil, D.; Patil, P.; Subramanian, V.; Joy, P. A.; Potdar, H. S. Highly sensitive and fast responding CO sensor based on Co_3O_4 nanorods. Talanta 2010, 81, 37-43.

(9) Chen, K. W.; Tsai, J. H.; Chen, C. H. NiO functionalized Co_3O_4 hetero-nanocomposites with a novel apple-like architecture for CO gas sensing applications. Mater. Lett. 2019, 255, 126508.

(10) Chen, K. W.; Tsai, J. H.; Chen, C. H. Controlled synthesis and CO sensing potentials of size-tunable highly-uniform mesoporous Co_3O_4 nanospheres. J. Alloys Compd. 2020, 816, 152524.

(11) Dou, Z. F.; Cao, C. Y.; Chen, Y.; Song, W. G. Fabrication of porous Co_3O_4 nanowires with high CO sensing performance at a low operating temperature. Chem. Commun. 2014, 50, 14889-14891.